City Research Online

City, University of London Institutional Repository

Citation: Li, Y., Yan, S., Shi, H., Ma, Q., Dong, X. & Cao, F. (2024). Wave load characteristics on a hybrid wind-wave energy system. Ocean Engineering, 294, 116827. doi: 10.1016/j.oceaneng.2024.116827

This is the accepted version of the paper.

This version of the publication may differ from the final published version.

Permanent repository link: https://openaccess.city.ac.uk/id/eprint/32410/

Link to published version: https://doi.org/10.1016/j.oceaneng.2024.116827

Copyright: City Research Online aims to make research outputs of City, University of London available to a wider audience. Copyright and Moral Rights remain with the author(s) and/or copyright holders. URLs from City Research Online may be freely distributed and linked to.

Reuse: Copies of full items can be used for personal research or study, educational, or not-for-profit purposes without prior permission or charge. Provided that the authors, title and full bibliographic details are credited, a hyperlink and/or URL is given for the original metadata page and the content is not changed in any way.

City Research Online: http://openaccess.city.ac.uk/ publications@city.ac.uk

Wave Load Characteristics on a Hybrid Wind-Wave Energy System

Yanni Li[a], Shiqiang Yan[b], Hongda Shi[a,c], Qingwei Ma[b], Xiaochen Dong[a,c], Feifei Cao[a,c*]

[a] Department of Ocean Engineering, College of Engineering, Ocean University of China, Qingdao 266404, China

[b] School of Science & Technology, City University of London, London EC1V 0HB, United Kingdom

[c] Shandong Provincial Key Laboratory of Ocean Engineering, Ocean University of China, Qingdao 266100, China

[*] Corresponding author. Department of Ocean Engineering, College of Engineering, Ocean University of China, Qingdao 266400, China. E-mail address: caofeifei@ouc.edu.cn

Abstract

Following the development of offshore wind turbine (OWT) systems and wave energy converters (WECs), there is an increasing demand for the development of hybrid systems that combine OWTs with WECs, for the purpose of reducing the Levelized Cost of Electricity (LCOE) of WECs by sharing foundations, increasing overall power output, and optimizing the utilization of marine space. One of the hybrid systems integrates WECs with the most widely adopted foundation used by existing wind farms, i.e. the fixed monopile foundation. While existing research mainly focuses on the characteristics of loads and power performance of WECs, the corresponding characteristics related to wave load on the monopile foundation and the hybrid system play a critical role in securing the safety and stability of the monopile foundation but is limited in the available literature. This paper presents an analysis of wave load characteristics on a fixed monopile foundation of a 15 MW OWT integrated with a torus-shaped heaving WEC using the ANASYS-Aqwa adopting the linear potential theory. The structure is subjected to regular and irregular waves in the operational sea conditions. The power take-off (PTO) system of the WEC is modelled by applying a linear damping in the present numerical work. The results suggest that the PTO damping has an insignificant impact on the wave load statistics. It is further confirmed that, the integrated WEC effectively reduces the wave load and overturning moment acting on the monopile foundation within a wide range of wave conditions. Moreover, the presence of the monopile also reduces the horizontal wave load on the WEC. However, the overall load on the hybrid system, which is the resultant force of horizontal wave force acting on buoy and monopile, is higher than that experienced by the monopile foundation of the OWT prototype. To the best of our knowledge, this is the first work investigating into the effect of integrated torus-shaped WECs on wave loads affecting fixed foundations. The findings offer valuable insights for the design and deployment of such hybrid systems in the near future.

Keywords: Hybrid wind-wave energy system; Wave load; Monopile foundation; torus-shaped Point-absorber; Potential theory

1. Introduction

The ongoing escalation of climate change-induced catastrophic consequences has urged the worldwide governments to prioritise a transition to net-zero economy by 2050. To enable this transition in an environmentally and economically viable (sustainable) manner, renewable energy sources are demanded to be exploited to replace fossil fuels. Internationally, offshore wind and marine resources are abundant. These considerations have brought the offshore wind and wave sectors to the forefront of research and development (R&D), contributing to the 'green industrial revolution'. Among these, the R&D of hybrid systems combining offshore wind turbines (OWTs) and wave energy converters (WECs) is one of the research focuses. The main aims of developing the hybrid system include maximising the energy output, optimising the use of marine space, reducing the cost by sharing the foundation/mooring, reducing the wave load on the WTs and/or suppressing the motion of the floating platform through installing WECs. Some recent literatures are summarised in Table 1.

Table 1: Recent literatures on hybrid wind-wave systems

Platform/Foundation	Point Absorber	OWC
Monopile	Homayoun et al. (2019), Ren et al. (2018), Khatibani et al. (2022)	Perez-Collazo et al. (2019), Zhou et al. (2020), Cong et al. (2021), Li et al. (2022)
Semi-Submersible	Lee et al. (2017), Hu et al. (2020), Chen et al. (2020), Wang et al., (2020), Kamarlouei et al. (2020), Si et al. (2021), Kamarlouei et al. (2022), Wang et al. (2022), Li et al. (2022)	Aubault et al. (2011), Zhu et al. (2019), Sarmiento et al. (2019), Zhang et al. (2022)
Spar	Muliawan et al.(2013a), Muliawan et al. (2013b), Li et al. (2018), Zhao et al. (2021) Yue et al. (2020), Wan et al. (2020)	Falcão et al. (2012), Oikonomou et al. (2021), Abazari et al. (2023), Li et al. (2022)
TLP	Ren et al. (2020), Rony et al. (2022)	Konispoliatis et al. (2021)
Barge	-	Aboutalebi et al. (2021a), Aboutalebi et al. (2021b)

Most existing wind farms operate on sites with the water depth below 30–35 m and apply bottom-fixed monopile foundations (Arany et al.,2018). As summarised in Table 1, both the point-absorber (Homayoun et al., 2019; Ren et al., 2018; Khatibani et al., 2022) and the oscillating water column (OWC, Pere-Collazo et al., 2019; Zhou et al., 2020; Cong et al., 2021; Li et al., 2022) devices have been integrated with OWTs adopting a fixed monopile foundation, yielding fixed wind-wave hybrid systems. The appearance of the monopile in close proximity significantly affects the characteristics of the loading on and the responses of the WECs, and consequently the power performance of the WECs. This has been investigated by using both the numerical and experimental studies in the literatures cited in Table 1. In turn, the integrated WECs are expected to affect the loading on the monopile that is closely related to the stability and fatigue life of the monopile. Therefore, the characteristics of the loading on WEC, OWT and the hybrid system is critical for the development and optimal design of the hybrid system. However, such characteristics is rarely seen in the available literature for fixed wind-wave hybrid systems. To the best of our knowledge, only Zhou et al. (2020) reported that an OWC can reduce the wave load on the monopile where the OWC is integrated with. Although direct evidences were not provided, Zhou et al. (2020) concluded that the wave reduction is caused by the effect of the OWC shell on redistributing the wave potential around the monopile, and the viscous drag and the flow separation

generated within the OWC chamber. The corresponding research on the effect of WECs on the characterises of the load on and the responses of the floating OWTs (FOWTs) in the floating wind-wave hybrid systems is more popular, as summarised in Table 1, although the hydrodynamic interaction between WECs and OWTs in the floating hybrid systems is more complex than that in the fixed hybrid systems. Arguably, recent research in this catalogue was driven by the need of suppressing the motion of the FOWT platform (motion mitigation) to improve the power performance of the wind turbine. To this end, the on-board point absorbers have shown their capacity in mitigating the motion of the FOWT platforms, including the semi-submersibles (Hu et al. ,2020; Chen et al., 2020; Si et al., 2021; Wang et al., 2022; Li et al., 2022; Kamarlouei et al., 2020, 2022), the spar (Muliawan et al., 2013a,b; Li et al.,2018; Yue et al., 2020 and Zhao et al., 2021), and the tension-leg platform (TLP, Ren et al., 2020; Rony et al., 2022). OWCs have also demonstrated their effectiveness on suppressing the motions of barge-type (Aboutalebi et al., 2021a, b) and semi-submersible (Zhu et al., 2019; Zhang et al., 2022) FOWT. Due to the mutual relationship between the loading on and the responses of the floating bodies, this type of research is often accompanied with the corresponding load characteristics. For example, Hu et al. (2020) found that the coupled multiple cylindrical heaving buoys increase the horizontal force harmonics on FOWT adopting WindFloat semi-submersible platform in a wide range of frequencies but reduce the maximum horizontal force and pitch moment on the FOWT platform. In addition, existing researches further concluded that the effects of the on-board WECs on influencing the dynamics of the FOWT depends on the configurations of WECs. With purposedly-tuned configuration, the WECs can control the platform motions (Kamarlouei et al., 2022); otherwise, OWC may have limited influence on the dynamics of the FOWT (e.g. Sarmiento et al., 2019). One critical configuration of WECs is the power-take-off (PTO) system. In this aspect, Si et al. (2021) combined a 5 MW DeepCWind semi-submersible FOWT with three WaveStar WECs and revealed that the PTO control strategy of WEC significantly influences the dynamics of platform and the power performance of the FOWT. They observed that, in general, the reactive control worsens the platform motion responses, whereas the spring-damping control mitigates the pitch motion; Zhang et al. (2022) have also attempted different PTO control strategies for the OWC WECs coupled with a DeepCWind FOWT, and found that the designed gain scheduling control schemes can reduce 15% platform pitch motion and 6% tower base fatigue load.

As discussed above, WECs in the floating hybrid system may significantly affect the motion of the floating platform and thus the power performance of the OWT. This brings challenges in system optimisation and control. However, WECs in the fixed hybrid system does not bring considerable effect on the power performance of the OWT, the control systems of WECs and OWT are less dependent on each other. For this reason, this paper contributes to the development of a fixed wind-wave hybrid system, in which a torus-shaped heaving buoy with a fixed monopile OWT. The concept of the hybrid system has been proposed by Ren et al (2018), who have carried out both experimental and numerical analysis on the power performance of the system at a model scale. However, the corresponding investigation on the wave load characteristics has not been done, resulting in uncertainties on the safety of the monopile foundation if WEC is installed. Following the work done by Zhou et al. (2020), the torus-shaped heaving buoy is also expected to diffract the wave field and consequently reduce the diffraction force acting on the monopile. But it is not clear whether the motion of the buoy would amplify or suppress the load on the monopile. Unlike the hybrid system proposed by Zhou et al. (2020), in which the OWC is fixed on the ground and therefore the load on the OWC will not be transferred to the monopile, the heaving buoy may need attach to the monopile. This means that the load on the buoy may also be transferred to the monopile. To this end, it is essential to consider the total load on the

monopile including the wave-induced load on the monopile and that transferred from the buoy. This is the second research question to be answered. Furthermore, although the loading characteristics on the floating hybrid systems cannot be directly applied to the fixed hybrid systems due to the distinguished different feature of the dynamic responses of the OWT foundations, some valuable conclusion, e.g. the effect of the PTO on the loading characteristics, can benefit the present study. In this work, the effect of the PTO of the OWC on the loading characteristics will be explored, yielding the third research question in this work. These questions have not been answered in the available literature on fixed wind-wave hybrid systems. Finally, Considering the up-scaling trend of the OWTs, the IEA wind 15 MW reference wind turbine (Gaertner et al., 2020), instead of the NREL 5 MW wind turbine used in Ren et al (2018), is chosen to provide the porotype of the monopile foundation and to design the torus-shaped buoy. From the existing research on floating hybrid systems, we regret the potential significance of the structural responses to the loading characteristics, but it is ignored in this paper for simplification. The appropriation of ignoring the structural responses, i.e. the vibration of the monopile, can be partially justified by the fact that only the operational sea conditions are considered in this work and the structural vibration may be minimal in such a condition. Further work will follow in the near future when the survivability and the breaking wave impact on the hybrid system are investigated. The findings of this work are expected to offer valuable insights for the design and deployment of such hybrid systems in the near future.

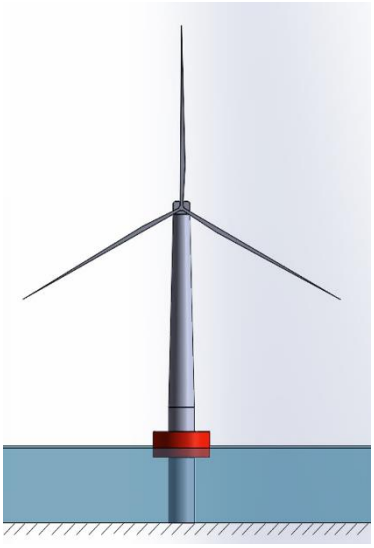

Fig. 1. Concept of the hybrid wind-wave system

2. Numerical specification and validation

2.1. Conceptual design and numerical model

Figure 1 illustrates the conceptual design of the present wind-wave hybrid system, consisting of a heaving buoy and fixed monopile foundation recommended by the IEA 15 MW reference OWT system. Following the technical specification defined by the reference turbine (Gaertner et al., 2020), the diameter of the monopile D_m is taken as 10 m and the mean water depth h is 30 m. The heaving buoy has a torus shape. It is only allowed to move vertically along the monopile through the linear guide-roller system (Ren et al., 2018) to extract wave energy and its horizontal movement is constrained. A hydraulic system equipped between buoy and monopile can supply linear and Coulomb damping (Zhao et al., 2021) and is used to approximate the PTO system. Referring to the WEC dimensions in Ren et

al. (2018), which states that the external diameter is twice of the internal diameter, and the height is equal to the internal diameter, the external (D_o) and internal (D_i) diameters of the buoy in this paper are set to 22 m and 11 m, respectively. The height H_b and draft d of the buoy are 11 m and 4.5 m, respectively~~, yielding a centre of gravity at 1 m above the mean sea level (MSL)~~. The mass of the buoy is configurated to ensure the hydrostatic equilibrium. In this work, the buoy is constrained to have only one degree of freedom in heaving, and therefore, the hydrodynamic stability subjected to a small rotation does not need to be considered, unlike other isolated point absorber devices floating in the water with 6 degrees of freedom. For this reason, we consider a uniform mass distribution and therefore the centre of gravity is placed at 1 m above the mean sea level (MSL). It shall be noted, if the buoy floats in the sea with the constraint of the monopile and subjected to 6 degrees of freedom, such high centre of gravity may cause hydrodynamic instability.

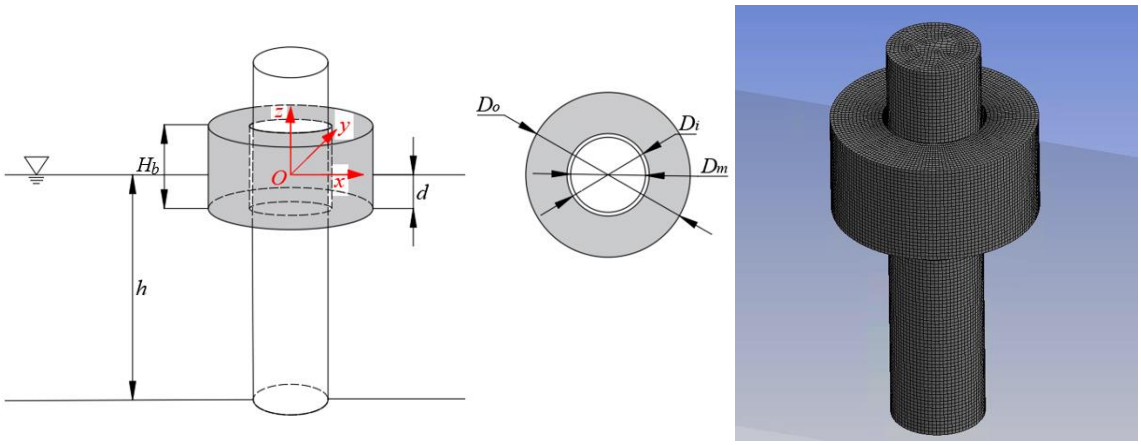

(a) (b)

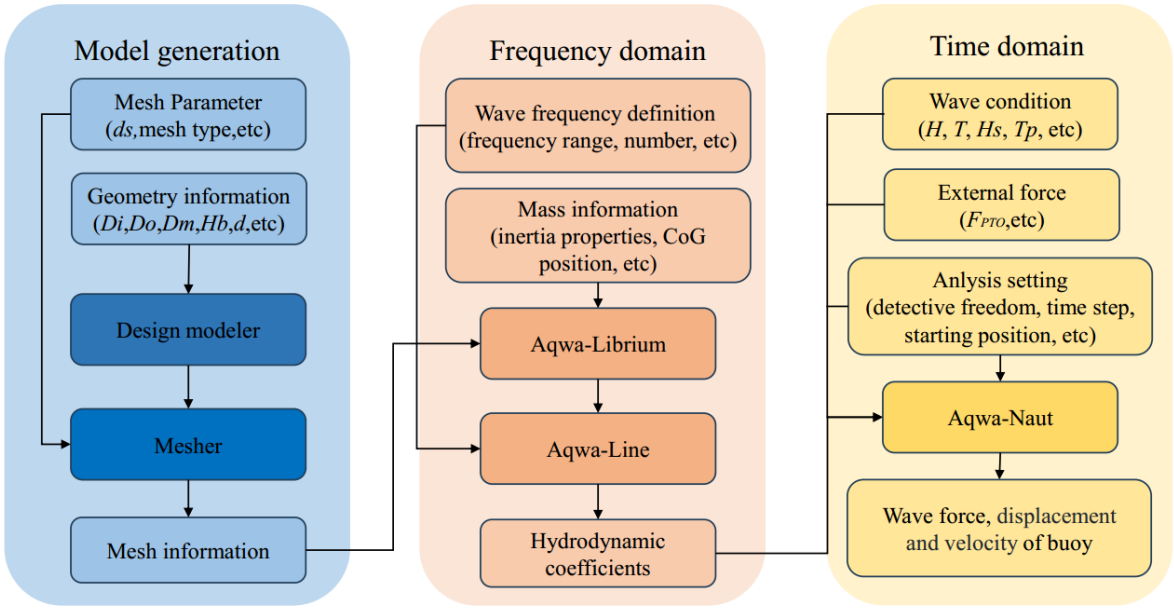

(c)

Fig. 2. Sketch of the monopile and buoy (a), the illustration of the mesh (b) and numerical modelling flowchart

As indicated above, the hydro- and aero-elasticity of the structure are ignored, consequently all components of the hybrid system are assumed to be rigid in this work. To this end, the aerodynamics

of the blade, hub and tower does not affect the hydrodynamics of the foundation. With this assumption, the wind-wave hybrid system illustrated in Fig. 1 is simplified by two rigid bodies, i.e. the buoy and the monopile, sketched in Fig. 2 (a). The seabed is simplified as a flat bed. We adopt the ANASYS-Aqwa which is based on the linear potential theory in which the fluid is assumed to be incompressible, inviscid and irrotational, linearised free surface and body surface boundary conditions are implemented. ANASYS-Aqwa can compute the hydrodynamic load/coefficients on floating or fixed rigid bodies by employing linearized three-dimensional radiation/diffraction theory in either frequency or time domain. The details on the ANSYS-Aqwa and its applications to the hydrodynamic statistics on multiple bodies can be found in Si et al. (2021), Ren et al. (2020), and Ghafari et al. (2022), only a brief of the procedure used for the simulation in this work is given herein.

In the ANASYS-Aqwa simulation, the monopile is set to be fixed by a rigid joint that connects to the central point of the bottom of the monopile to the seabed. The buoy is restricted to have one degree of freedom in heave. A full-scale model is used in the simulation. The frictional resistance between the heaving buoy and the monopile is neglected because the linear guide-roller system has a very low friction effect (Ren et al., 2018). A cartesian coordinate system *Oxyz* is defined with the origin located at the centre of the monopile and in line with MSL, as shown in Fig. 2 (a). The mesh of monopile and buoy is shown in Fig. 2(b). As shown in the numerical modelling flowchart in Fig. 2(c), in addition to using the Design Modeler and Mesher modules for preprocessing, which include modelling and meshing, the numerical procedure consists of two phases. In the first phase, the hydrodynamic coefficients, including the added mass and damping coefficients on the monopile and the buoy are estimated using the frequency-domain analysis module, i.e. Aqwa-Line, which employs the linearized three-dimensional radiation/diffraction theory. After the hydrodynamic coefficients (radiation and diffraction) are obtained in the first phase, a time-domain simulation is followed using Aqwa-Naut module. The memory effect of the radiation force is taken into account through the convolution approach in the time domain.

In the frequency-domain linear potential theory, the total potential $\varphi(\vec{X})$ with a specific exciting frequency ω at a position $\vec{X}$ is written as a linear superposition of different components (ANSYS, 2020),

$$\varphi(\vec{X}) = \varphi_I + \varphi_d + \sum_{n=1}^{N}\sum_{j=1}^{6}\varphi_{rjn}x_{jn} \quad (1)$$

where φ_I and φ_d are the isolated space dependent incident wave potential and the corresponding diffraction wave potential; $x_{jn}$is the amplitude of the motion of the *n*-th structure in the *j*-th motion component (i.e. surge, sway, heave, pitch, roll and yaw); φ_{rjn} is the unit radiation potential corresponding to x_{jn} while other structures remain stationary; *N* is the number of structure involved in the system, which is 2 in the present work. The incident wave potential φ_I is specified by a wave theory. In this work, the second order Stokes wave theory is used to specify the incident wave potential. Preliminary investigation has confirmed such wave theory is sufficient for describing the incident wave in all cases considered in this paper. φ_d and φ_{rjn} are obtained by solving the corresponding Laplace equations with linearized free surface and body surface boundary conditions.

Add the Laplace's equation and the boundary conditions here

After the velocity potentials are solved, the corresponding force components can be obtained by integrating the velocity potential over the wetted structure surface, *son*,

$$F_{I,jn} = -i\omega\rho \int_{Son} \varphi_I n_{jn} ds \quad (2)$$

$$F_{d,jn} = -i\omega\rho \int_{Son} \varphi_d n_{jn} ds \quad (3)$$

$$F_{rjn,kl} = -i\omega\rho \int_{Son} \varphi_{rjn} n_{jn} ds \quad (4)$$

where F_I is the Froude-Krylov force, i.e. the unsteady pressure force resulted from the undisturbed incident wave; F_d is the diffraction force brought by the reflected wave from the wetted structure surface; j and n in the subscript stand for the same meaning as Eq. (1); $F_{rjn,kl}$ is the radiation force acting on the n-th structure due to the radiation wave induced by the k-th motion components of the l-th structure; ρ is the density of the fluid . The radiation potential can be expressed in real and imaginary parts and substituted into Eq. (4) to produce the added mass and damping coefficients, i.e. $A_{rjn,kl}$, $B_{rjn,kl}$, respectively:

$$A_{rjn,kl} = \frac{\rho}{\omega} \int_{Son} \mathrm{Im}[\varphi_{rjn}] n_{jn} ds \quad (5)$$

$$B_{rjn,kl} = -\rho \int_{Son} \mathrm{Re}[\varphi_{rjn}] n_{jn} ds \quad (6)$$

Overall, the total wave-induced force can be obtained by

$$F_{jn} = F_{I,jn} + F_{d,jn} + \sum_{l=1}^{N} \sum_{k=1}^{6} F_{rjn,kl} \quad (7)$$

After the force on and the acceleration of the floating body are sought, ~~integrating the acceleration results in the displacement of the floating body, i.e. x_{jn} in Eq. (1),~~ the Laplace equations and boundary conditions for radiation potentials can be solved. After that, Eqs. (2-7) are used to find the hydrodynamic coefficients for both the monopile and the buoy that will be used in the 2nd phase that evaluates the time-domain force on the buoy and the monopile, and solves the motion equation of the buoy using Newton's 2nd Law,

$$\big(m_1 + A_{11}(\infty)\big)\ddot{z}(t) + \int_0^t k_{11}(t-\tau)\dot{z}(\tau)d\tau + R_1 z(t) = F_{e1}(t) - F_{PTO}(t) \quad (8)$$

where m_1 is the mass of the heaving buoy, z is the displacement of the buoy, $A_{11}(\infty)$ is the infinite-frequency added mass, $k_{11}$is the velocity impulse function, and F_{e1} is wave exciting force which is made up of the Froude-Krylov force and diffraction force. The convolution integral $\int_0^t k_{11}(t-\tau)\dot{z}(\tau)d\tau$ represents the memory effect of the radiation force and k_{11} can be obtained by Eq. (9).

$$k_{11}(t) = \frac{2}{\pi} \int_0^{\infty} B_r(\omega)\cos(\omega t) d\omega \quad (9)$$

The hydrostatic stiffness coefficient of buoy is presented in the following equation:

$$R_1 = \pi\rho g\big(D_o^2 - D_i^2\big)/4 \quad (10)$$

The PTO force F_{PTO} is approximated using

$$F_{PTO}(t) = -B\dot{z}(t) \tag{11}$$

where B is the PTO damping coefficient, $\dot{z}(t)$ is the heaving velocity of the buoy.

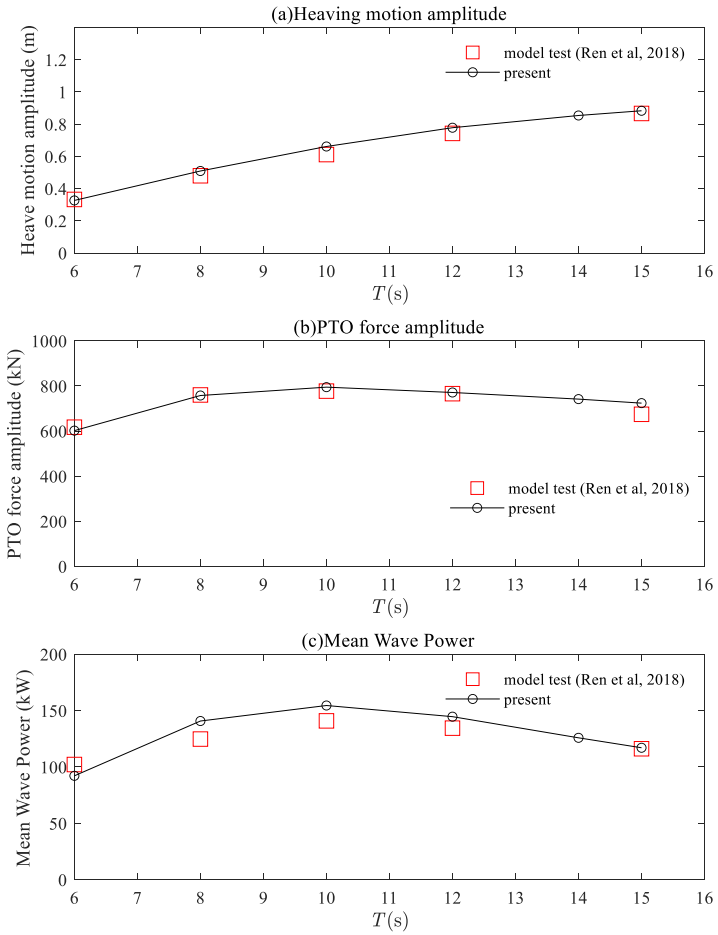

Fig. 3. Comparison of (a) heaving amplitude, (b) PTO force amplitude and (c) Mean wave power in the cases with different wave periods (H = 2 m)

It is worth noting that the theoretical assumption of the linear potential theory limits its application to complex fluid-structure interactions involved in the wave interaction with the present hybrid system, such as the small-scale viscous and turbulent effects, the breaking wave and slamming, aeration and flow separation, the gap resonance between the buoy and monopile foundation. Considering the fact that the WEC would only operate in a normal sea state where the breaking wave, slamming, and aeration are not significant. Under the extreme condition, the WEC stops operating and the whole system behaves similarly to a fixed step cylinder, existing research on breaking wave impacts on offshore structure would give a good reference to the evaluation of the extreme load. We focus on the operational condition without current in this paper covering a wide range of wave conditions. Although the viscous effects can be taken into account through adding an artificial viscous term in the motion equation of the floating bodies (e.g. Muliawan et al., 2013 ab; Lee et al., 2018; Hu et al., 2020; Si et al., 2021; Li et al., 2022), it is ignored in the present ANSYS-Aqwa simulations, as many existing research on the hybrid wind-wave system developments (e.g. Zhao et al., 2021; Ren et al., 2018, 2020; Homayoun et al., 2019; Gkaraklova et al., 2020; Khatibani and Ketabdari, 2022). Further comparison with the CFD results will

be presented to analyse the significance of the viscous effect. Regarding the gap resonance between the buoy and the monopile, the viscous effect may only be significant near the resonance region and does not influence the qualitative conclusion (Ekerhovd et al, 2021). Extra attention is paid in this paper to compare our numerical results with experimental data and computational fluid dynamics (CFD) results in the following section.

2.2. Numerical Validation

In order to validate the present numerical approach, the experimental data from Ren et al. (2018) is used. In this experiment, a monopile OWT with a heaving-type WEC was tested subjected to a series of wave conditions. A 1:50 scaling is used in the experiment. In the model scale, the water depth is 0.3 m, the monopile diameter is 0.12 m, the outer and inner diameter of the buoy are 0.32 and 0.16 m, respectively; The height and the draft of the WEC are 0.16 m and 0.06 m, respectively. A linear guide-roller system is set between the buoy and the monopile and a vertical guide is introduced to allow the motion of the buoy in heaving only. The PTO force in this work is taken as $B_{PTO}\dot{z}(t)|\dot{z}(t)|$ where the quadric PTO damping coefficient is taken as 0.8 kNs^2/m^2. The viscous effect is neglectable in the present numerical simulation. The wave power captured by the WEC can be estimated by multiplying the PTO damping force and the heaving velocity of the buoy. In the present numerical work, a full-scale model is used. Fig. 3 compares the present results with the experimental data in terms of the heaving amplitude of the buoy, PTO force amplitude and the mean wave power taken by the buoy in the cases with different wave periods ranging from 6 s to 15 s. The data shown in Fig.3 correspond to the full-scale value and the wave height is kept to be constant, i.e. 2 m. This figure shows a satisfactory agreement between the present numerical results and the experimental data by Ren et al. (2018), especially the PTO force. The motion response and the mean wave power are slightly overpredicted.

As discussed in the Introduction and shown in Fig. 3, the experimental and numerical work conducted by Ren et al. (2018) did not cover the load characterises on the monopile. Although the satisfactory agreement between the present numerical results using ANSYS-Aqwa can justify the applicability of the present numerical model, additional comparison with CFD results is also made for further verification and analysis of the viscous effects. For this purpose, the CFD software Flow3D is used. For both the Flow3D and the present ANSYS-Aqwa modelling, the full-scale hybrid system illustrated in Fig. 1 and Fig. 2 are used. The wave height H is 1 m and the wave period T is 9 s, yielding a kh value of 1.6 where k is the wave number. As will be shown in the following section, this wave condition is the most critical condition leading to a maximal wave load on the monopile foundation. The heave displacement of the buoy and the horizontal force on the monopile foundation are plotted in Fig. 4 for comparison. In this figure, the horizontal force acting on the monopile F_x is nondimensionalised by $\rho g A D_m^2$ where g is the gravitational acceleration, A is the incident wave amplitude. As observed, the time histories of the heave displacement (Fig. 4(a)) and the horizontal force (Fig. 4(b)) resulted from the present ANSYS-Aqwa are close to the corresponding CFD results. This implies that the viscous effect is insignificant in the cases considered in this paper. This is further justified by the comparison of the pressure force and the viscous force obtained from the CFD simulation, i.e. Fig. 4(c) which shows that the viscous force is almost zero. This is consistent with the analysis of the Reynolds number in the cases considered in this paper that ranges from 5.3 to 22.8 $\times 10^6$ and suggests an insignificant viscous effect. To this end, we are confident that the present linear potential software ANSYS-Aqwa is valid for the load characteristics on the present hybrid system subjected to the wave conditions set in this paper. One may also agree that the use of linear potential theory has benefits on identifying different

types of the loads, e.g. the diffraction and radiation load, which are important in the design and optimisation stage, compare to the CFD modelling.

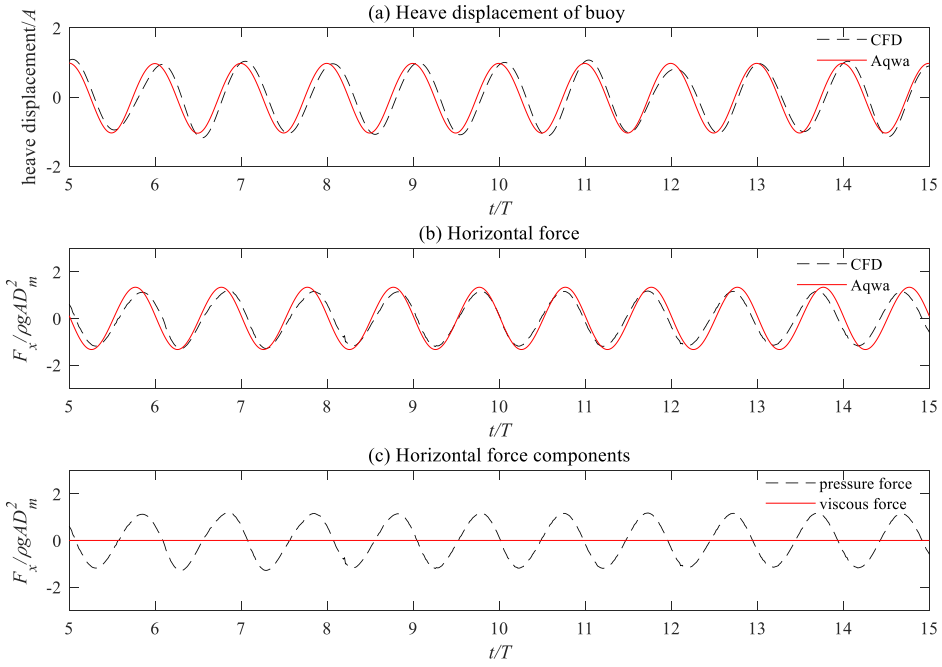

Fig. 4. Comparison of (a) heaving amplitude, (b) horizontal force on the monopile between the ANSYS-Aqwa and CFD simulations and (c) force components from the CFD modelling (H = 1 m)

3. Numerical Results and Discussions

On the basis of the numerical validation presented above, the present numerical approach is now used to characterise wave load acting on the hybrid wind-wave system outlined in Section 2.1. As stated in the Introduction, this paper aims to characterise the wave load subjected to operational conditions with a particular focus on the role of integrated WEC on reducing the wave load on the monopile. Based on the sea state around Shandong province in China (Hu et al., 2020), in the numerical investigation, the wave period T varies from 3 s to 13 s in the cases with regular wave and the peak period ranges from 4 s to 12 s in the cases with irregular wave. The significant wave height is taken as 1 m for both regular and irregular waves. For each wave condition, the wave load on the monopile with and without considering the WEC will be analysed and compared. For convenience of the analysis, the force and overturning moment on the monopile and the buoy are nondimensionalised by using $F/\rho gAD_m^2$ and $M/\rho ghAD_m^2$, respectively, where F and M are the amplitude of force and overturning moment; the dimensionless parameter kh is used to indicate different wave period (in the case with irregular wave, k corresponds to the peak wave frequency).

3.1 Mesh sensitivity and convergence

The convergence tests are carried out prior to the analysis of the wave load. For this purpose, different mesh sizes are used for the cases considered in this section. Fig. 2(b) illustrates the computational mesh used in the present numerical work with a maximum element size ds of 0.7 m and defeaturing tolerance of 0.4 m. For all mesh, the ratio of ds and the defeaturing tolerance is the same, i.e. 1.75. The heaving

RAO and the horizontal force acting on the monopile are considered as the criteria to assess the convergence. One example is presented in Fig. 5 for demonstration. In this case, the incident wave height H = 1 m and the period T = 7 s. Different values of ds ranging from 0.55 m to 3.96 m, yielding total numbers of cell ranging from 36428 to 892, are used. As observed from Fig. 5, the RAO of the buoy and the wave load acting on the monopile both converge to specific values when $ds \leq 0.7$ m (total number of cells is 24044). Similar observation is found for other cases, the results are not shown to save the space.

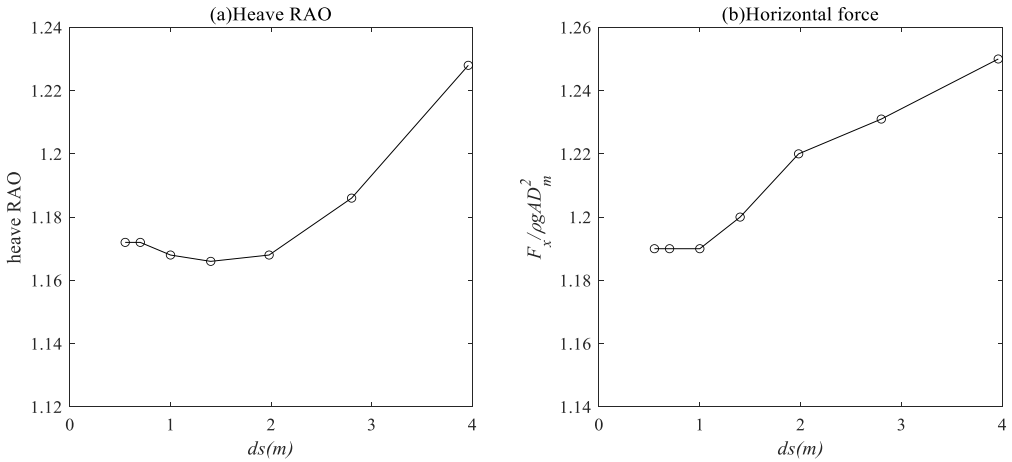

Fig. 5. Heave RAO and Horizontal force acting on the monopile in the cases with different mesh sizes (H = 1 m, T = 7 s)

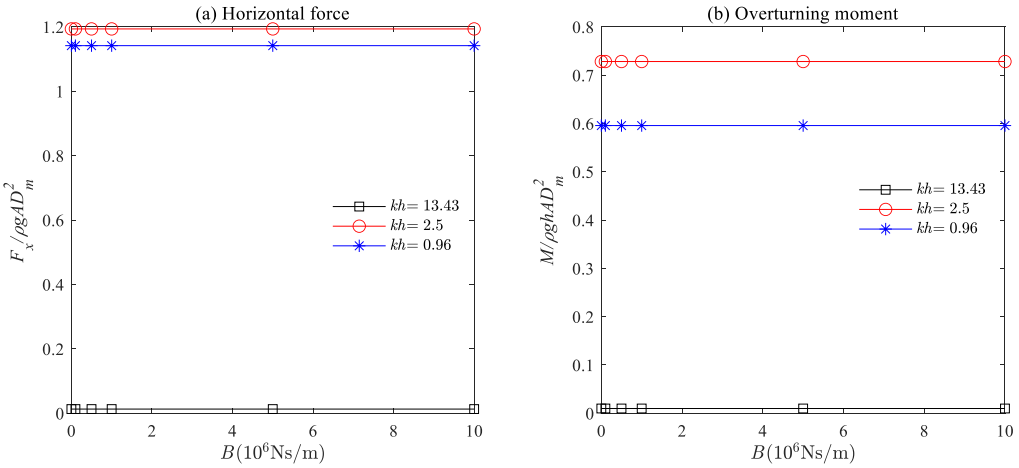

Fig. 6. Horizontal force and overturning moment acting on the monopile in the cases with different PTO damping (H = 1 m)

3.2 Sensitivity of PTO on Wave Load on Monopile

As discussed in the Introduction, the PTO of WECs may play a critical role in loading characteristics on the hybrid wind-wave system adopting FOWT (Si et al, 2021; Zhang et al., 2022), systematic investigations are carried out in this section to assess how the PTO affects the wave load on the monopile. For this purpose, Eq. (7) is used to model the PTO through imposing a damping force on the WEC. Different values of PTO damping coefficient B, ranging from zero to 10×10^6 Ns/m are used.

Figure 6 displays the horizontal force and overturning moment acting on the monopile in regular waves with different wave periods subjected to different PTO forces. The overturning moment is calculated using the central point of the cross-section of the monopile at the seabed. For clarity, only three wave conditions, i.e. kh = 14.32, kh = 2.5 and kh = 0.96 are plotted. The first condition represents a deep-water wave whereas the other two represent the wave in finite depth. These cases cover the entire range of wave conditions. It is observed from Fig. 6 that the horizontal wave load and overturning moment on the monopile are not sensitive to the PTO force. It is noted that the wave load on the fixed monopile mainly consists of Froude-Krylov force and diffraction force in the present investigation since the viscous effect is ignored. The former is relevant to the undisturbed incident wave and thus not affected by the PTO damping. The latter is influenced by the presence of the WEC, which behaves as a shield to the monopile (see Fig. 2). The PTO damping considerably affect the heaving motion of the buoy (the heave RAO of the buoy can be reduced from a maximum value of 1.66 to a small value close to zero), however, subjected to the operational wave condition (i.e. H = 1 m in the present investigation), the introduction of the PTO force does not produce a large reduction of the motion, i.e. at a maximum level of 1 m, and the area obscured by the WEC experiences minimal changes. Therefore, the PTO force does not considerably affect the diffraction force on the monopile. This may explain why the horizontal wave load and the overturning moment on the monopile are not sensitive to the PTO force. It is worth noting that the linearised viscous damping in the present study could be introduced in the numerical simulation with the same format of PTO force, e.i. $F_{vis} = -B_{vis}\dot{z}(t)$, where B_{vis} is the viscous damping coefficient. Therefore, Fig. 6 also could be used to illustrate the influence of viscous damping on horizontal force and overturning moment acting on the monopile in regular waves. The observation in Fig.6 further suggests that even a viscous damping in the heaving motion of the WEC is introduced in the present study, it is not expected to change the characteristics of the horizontal wave load and the overturning moment on the monopile.

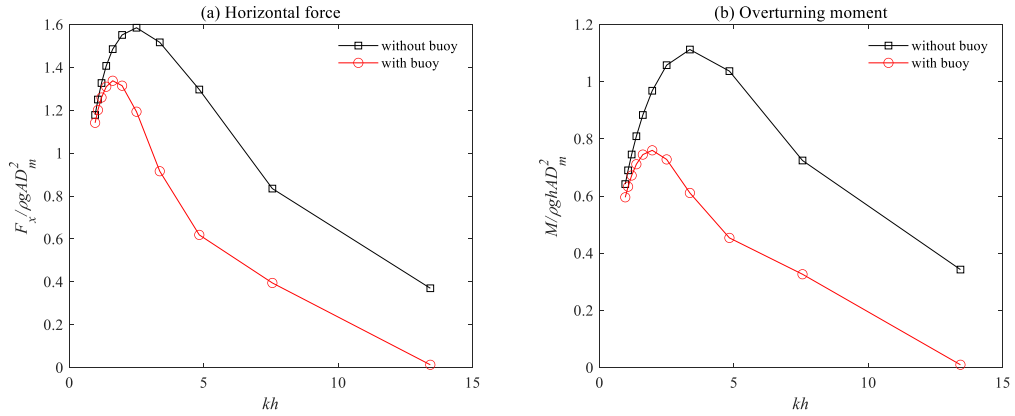

Fig. 7. Horizontal force and overturning moment acting on the monopile in the cases with different kh (H = 1 m, F_{PTO} = 0 N)

3.3 Regular wave load on monopile

Figure 7 compares the horizontal force and overturning moment acting on the monopile in the cases with and without the heaving-buoy WEC. Since the PTO damping of the buoy does not bring considerable effects on the loading on the monopile (Fig. 6), zero PTO force is used in the cases shown in Fig.7. As observed from Fig.7 (a), the dimensionless horizontal force increases as kh increases until a peak value appears (i.e. kh = 1.6 and kh = 2.5 for the monopile with and without buoy, respectively). After the occurrence of the peak value, it decreases as kh increases. A similar trend of variation is

observed in Fig. 7 (b) for the overturning moment acting on the monopile. This observation on the load reduction is in line with the effect of the OWC shell on monopile (Zhou et al., 2020). The peak value of the overturning moment occurs at kh = 1.965 and kh = 3.365 for the monopile with and without the buoy, respectively. More importantly, the presence of the buoy significantly reduces the wave load on the monopile within the whole range of the frequency considered in this paper. A further comparison of the force components, i.e. Froude-Krylov force and diffraction force, is shown in Fig. 8. As confirmed by Fig. 8, the Froude-Krylov force only depends on the undisturbed incident wave and thus the presence of the buoy does not change the Froude-Krylov force on the monopile. The load reduction on the monopile by the WEC is mainly caused by its effect on the diffraction force. The width of the gap between the buoy and the monopile is 0.5 m (Fig.2). As indicated above, the buoy behaves as a shield to the monopile near the free surface, where the wave action is more significant. Only the portion of the incident wave that transits through the buoy can reach the monopile surface covered by the buoy and result in the diffraction from this part of the surface. Longer wave, more significant wave can be transited through the buoy and therefore less 'shielding effect' is provided by the buoy. As observed from Fig. 8, when $kh \leq 4.834$ (corresponding wavelength is greater than 39 m, the reduction of the diffraction force by the WEC becomes more significant as kh increases (the wavelength decreases), because of less transited wave through the buoy. When the wavelength becomes close to or smaller than the buoy diameter, e.g. kh = 7.5 (wavelength is approximately 25 m) and kh = 13.4 (wavelength is approximately 14 m), the presence of the WEC amplifies the diffraction force. It is further found that in the cases with large kh ($kh \geq 4.834$), the WEC brings a considerable change in the phase of the wave load (Fig. 9). This can explain why the WEC reduces overall force on the monopile (Fig.7(a)), although the diffraction force is more significant when the WEC is introduced.

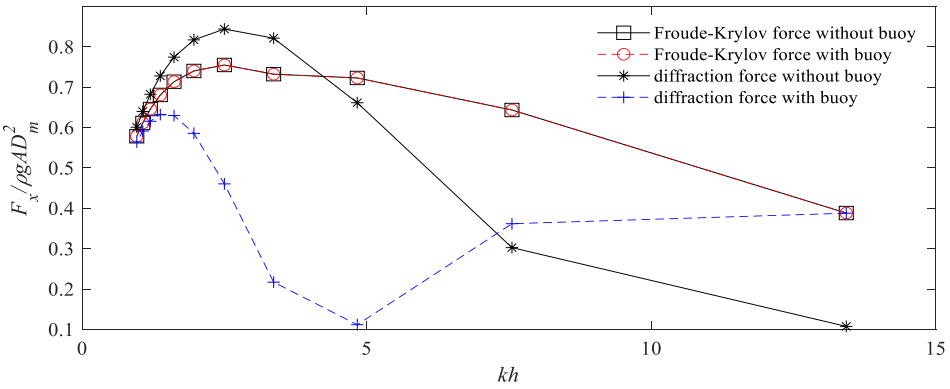

Fig. 8. Froude-Krylov force and diffraction force acting on the monopile in the cases with different kh (H = 1 m, F_{PTO} = 0 N)

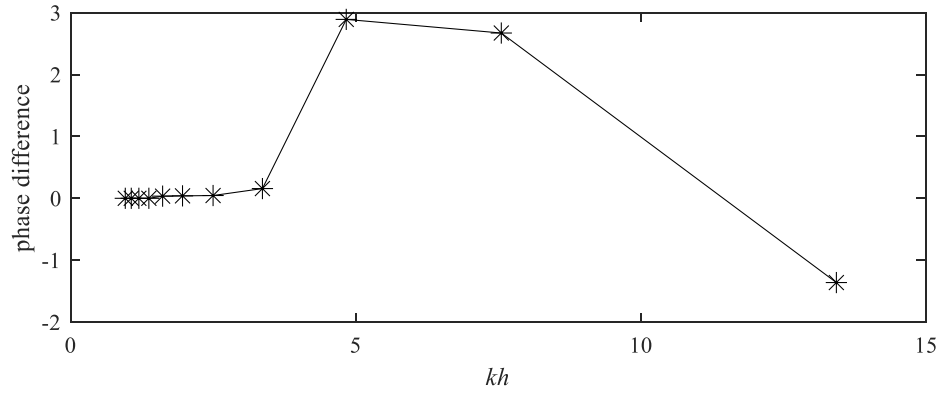

Fig. 9. Phase difference on the diffraction force on the monopile in the cases with different kh (H = 1

m, F_{PTO} = 0 N)

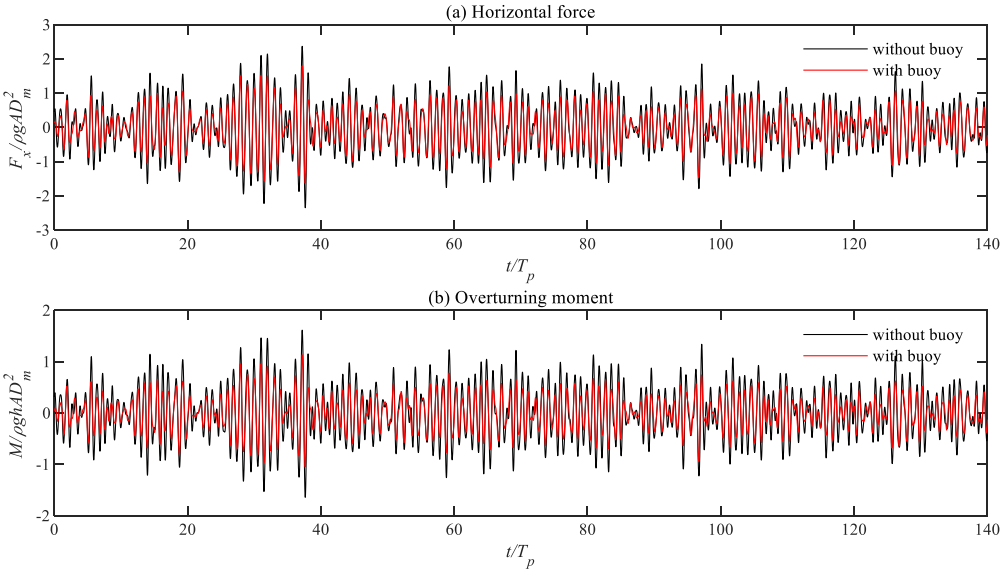

Fig. 10. Time histories of (a) horizontal force and (b) overturning moment acting on the monopile (H_s = 1 m, T_p = 7 s, F_{PTO} = 0 N)

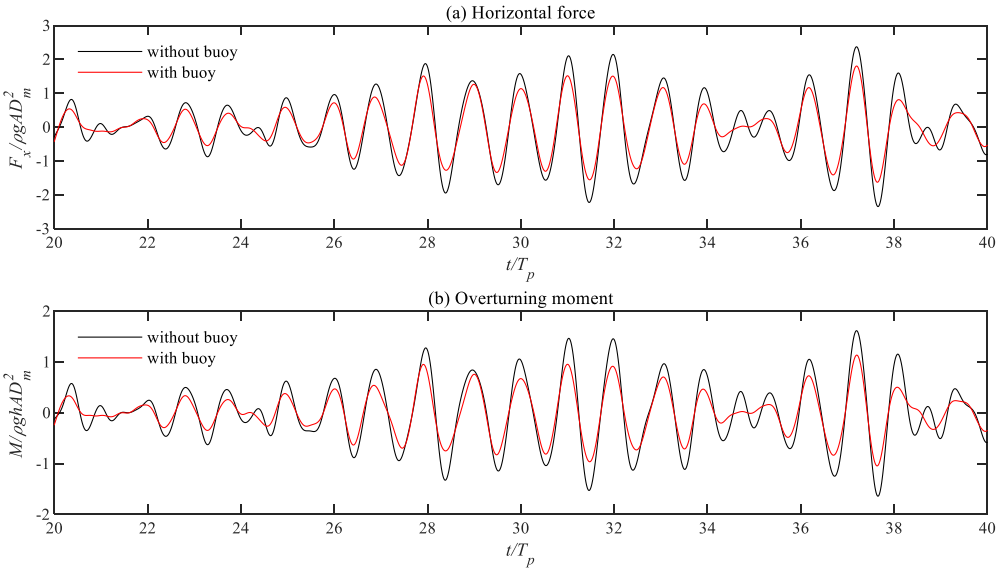

Fig. 11. Time histories of (a) horizontal force and (b) overturning moment acting on the monopile during the period with occurrence of maximin wave load (H_s = 1 m, T_p = 7 s, F_{PTO} = 0 N)

3.4 Irregular wave load on monopile

In the cases with irregular waves, the JONSWAP spectrum with the peak enhancement factor (γ) of 3.3 is applied in the present work. The peak period ranges from 4 s to 12 s and the significant wave height is taken as 1 m. For all cases with irregular wave, a random phase is assigned and the simulation is run for a sufficiently long duration leading to a smooth spectrum, e.g. 1000 s for the cases with the wave period of 10 s. Fig. 10 and Fig. 11 display the time histories of the horizontal force and the overturning moment acting on the monopile in the case with H_s = 1 m and T_p = 7 s. The corresponding *kh* value is 2.5. Similar to the cases with regular waves, the introduction of the buoy suppresses the wave load on the monopile, especially in terms of reducing the peak wave load. One may also notice that the buoy

does not bring considerable change on the phase of the wave load, although the phase on high-frequency wave components may be changed significantly as observed in the regular wave cases from Fig. 9. The corresponding amplitude spectra of the horizontal force and overturning moment are plotted in Fig. 12. Clearly, the amplitudes of horizontal force and the overturning moment corresponding to the entire frequency range are suppressed by the integrated buoy. Even for the high-frequency component with dimensionless frequency greater than 2.75 (corresponding to $kh \geq 4.834$ in Fig.8), the buoy suppresses the force/moment components. Similar to Fig. 7, the buoy slightly shifts the peak frequency to a lower position for both the horizontal force and the overturning moment by $0.0175\sqrt{g/h}$ and $0.022\sqrt{g/h}$, respectively; it significantly reduces the peak values by 25% and 32% for the horizontal force and overturning moment, respectively.

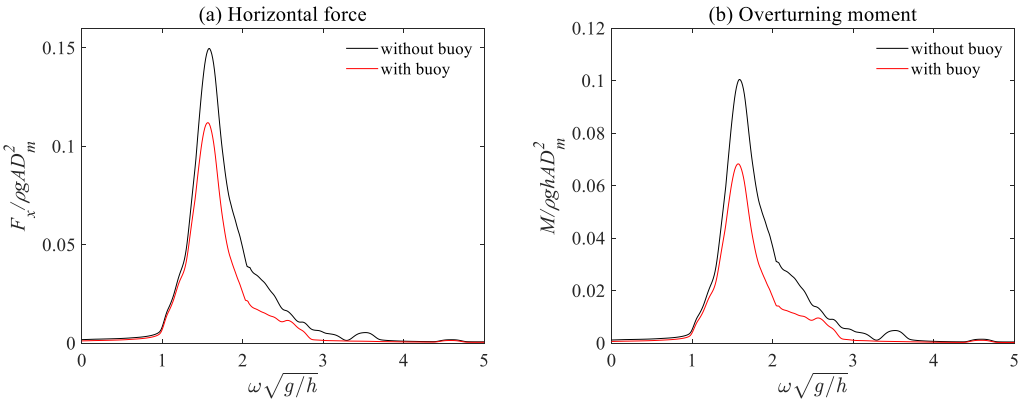

Fig. 12. Spectra of horizontal force and overturning moment acting on the monopile (H_s = 1 m, T_p = 7 s, F_{PTO} = 0 N)

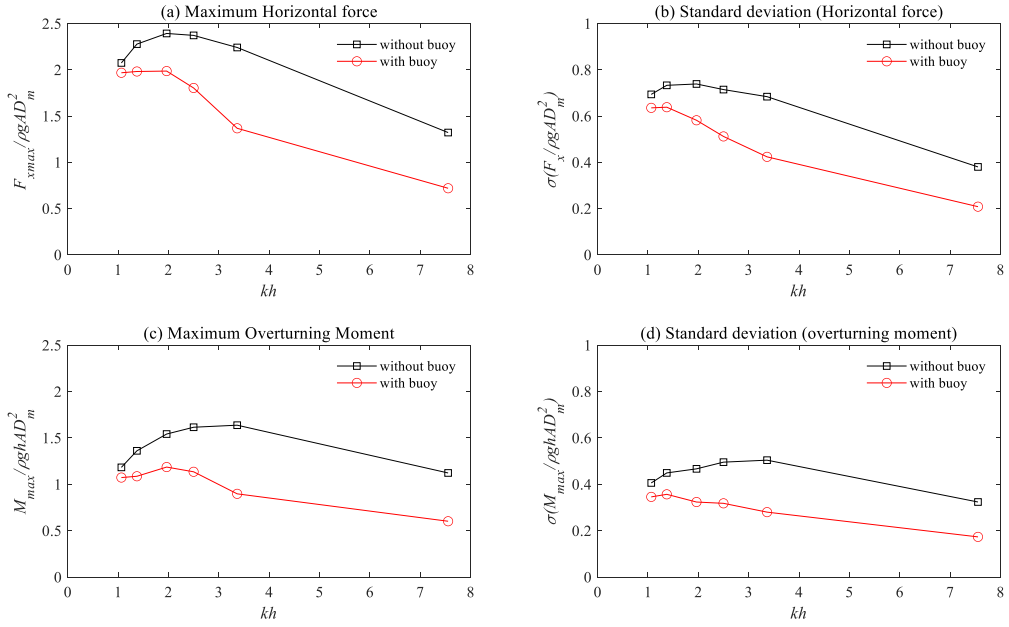

Fig. 13. Statistics on maximum value and standard deviation of horizontal wave load and overturning moment on monopile with and without buoy in irregular sea (H_s = 1 m, F_{PTO} = 0 N)

Similar phenomena are also observed in the cases with other peak frequencies. Statistically, the maximum wave load and the standard deviation are of interest for the structure's safety. Fig. 13 duplicates such statistic data in all irregular wave cases considered in this paper. For convenience, it is also given in terms of *kh* values. It is found that both the maximum value and the standard deviation of

the force/moment on the monopile are suppressed by the integrated buoy. The effect of the reduction become more significant as *kh* increases within the intermediate range (largely fall in the range of finite-depth wave, i.e. $kh \leq \pi$). It is consistent with the results from the regular-wave cases (Fig.7).

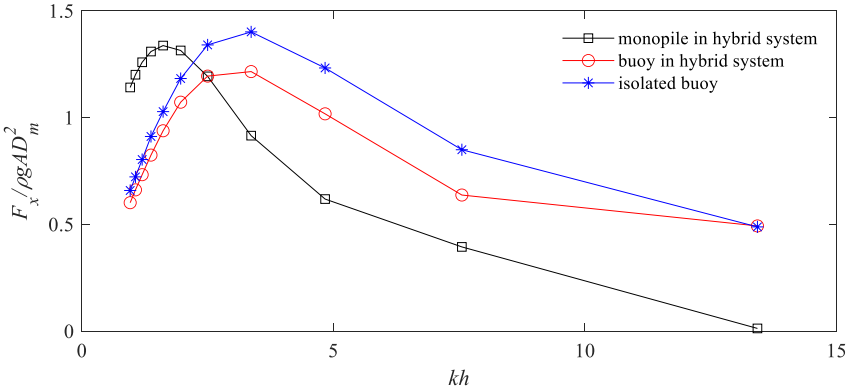

Fig. 14. Horizontal forces acting on the monopile and buoy in the cases with different *kh* (H = 1 m, F_{PTO} = 0 N)

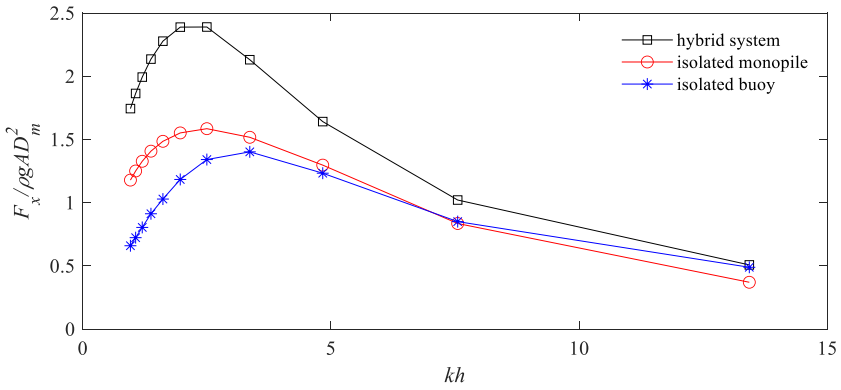

Fig. 15. Horizontal forces acting on hybrid system, isolated monopile and isolated buoy in the cases with different *kh* (H = 1 m, F_{PTO} = 0 N)

3.5 Wave load on hybrid wind-wave system

For the hybrid wind-wave system proposed in this paper, the heaving buoy is attached to the monopile. The load on the heaving buoy is transferred to the monopile through joint. Although the integrated buoy provides shielding effect on the diffraction force on the monopile, yielding a reduction of the load directly imposing on the monopile, one shall consider the overall load on the hybrid system during the design since the loads on the buoy are expected to be transferred to the monopile through joint.

Figure14 shows the horizontal forces acting on the monopile and the buoy for the hybrid system without considering the PTO damping. The data are abstracted from the regular-wave cases discussed in Section 3.3. For the purpose of comparison, the horizontal force acting on an isolated heaving buoy is also plotted together. Clearly, the presence of the monopile reduces the horizontal wave load on the buoy, except in the cases with extremely low or high wave frequencies in Fig.14, due to the hydrodynamic interaction with the monopile in close proximity which may result in negative radiation damping and significantly alter the loading characteristics (Yan et al., 2011, 2012). More importantly, the horizontal force acting on the buoy in the hybrid system is compatible to the force acting on the monopile, although the peak value occurs at the different wave condition, i.e. *kh* = 1.615 and *kh* = 3.365 for the monopile and buoy, respectively. The latter corresponds to the natural frequency of the heaving buoy. The overall

horizontal force acting on the hybrid wind-wave system, which is the resultant force of horizontal forces acting on the buoy and the monopile, is displayed in Fig. 15, together with the corresponding force acting on an isolated monopile and isolated buoy for comparison. As observed, the horizontal force acting on the hybrid system is considerably higher than that on an isolated monopile and that on an isolated buoy. It shall be noted that the PTO force of the buoy considerably affect the motion of the buoy, as confirmed by Fig. 16(a) that shows the variation of heave RAO in the cases with different PTO coefficients, however, the horizontal force on buoy seems not to be affected by the PTO system (Fig.16(b)).

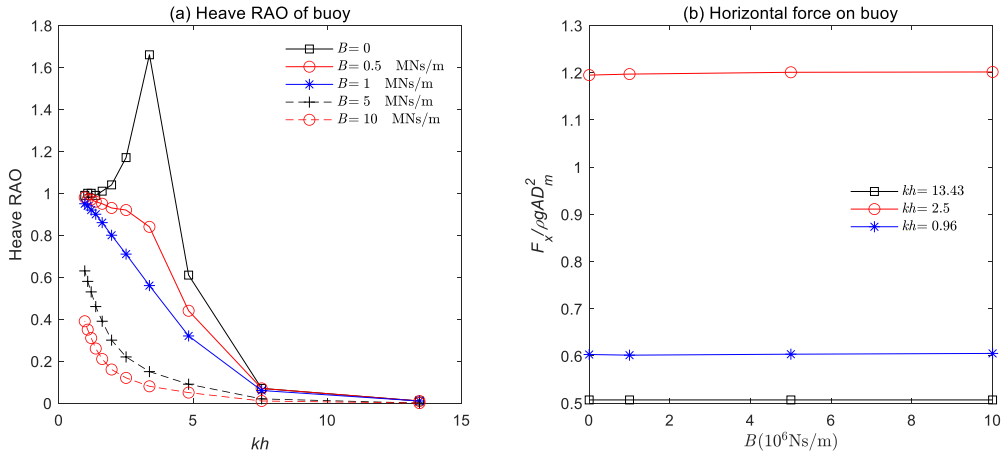

Fig. 16. Heave RAO of the buoy (a) and horizontal force on buoy of the hybrid system in the cases with different *kh* subjected to different PTO force (b) (H = 1 m)

4. Conclusion

In this paper, a conceptional design of a fixed wind-wave hybrid system is proposed to integrate a heaving buoy with the IEA 15 MW wind turbine with a fixed monopile foundation. A numerical model is established by using ANSYS-Aqwa. Necessary numerical validation and convergence investigation have suggested that the numerical approach is reliable for evaluating the wave load on the hybrid system under operational conditions. A systematic investigation is carried out by considering both regular wave and irregular wave conditions in a wide range of frequency. The results from the regular-wave cases reveal that the integrated buoy mainly provides a shielding effect and reduces the diffraction wave force on the monopile; the significance of the load reduction is not influenced by the PTO in the cases considered in this paper. In the sea state of irregular wave, the integrated buoy considerably reduces the maximum wave load and the standard deviation of the wave load on the monopile.

The present results suggest that the load on the overall hybrid system is generally more significant than the corresponding load on the isolated monopile without WECs. If the load on the buoy in the hybrid system needs to be borne by the monopile, the objective of load reduction by integrating the WEC may not be achieved. This may be different from the observation in the hybrid wind-wave system adopting FOWT. In the hybrid system adopting FOWT, the integrated WEC behaves as a damper, alters the natural frequency of the floating platform and consequently affects the dynamics of the platform. By tuning the PTO of the WECs, one can shift the natural frequency of the floating platform away from the operational condition of the hybrid system, and consequently, mitigate the motion and suppress the

wave load on the platform. Nevertheless, one may use an alternative system to withstand the wave load on the monopile, such as additional mooring, to reduce the overall load to be bearded by the monopile foundation. It is important to note some limitations of the present work, including (1) the linear potential theory applied in this paper is restricted by its assumption, high-fidelity computational fluid dynamic modelling will be done in the near future for revealing further details of the flow characteristics, including the turbulence and viscous effects, aeration; (2) only operational sea is considered. Under high sea state, violent wave breaking may occur, yielding impact load on the foundations or WECs; (3) the structural responses, i.e. the vibration of the monopile foundation, is not taken into account; and (4) the majority of the fixed offshore wind farm sit in a marine environment where wave and current co-exist. However, the current is ignored in the present research. These issues will be addressed in the near future.

Acknowledgment

The authors acknowledge the support from Shandong Provincial Natural Science Foundation (Grant No. ZR2021ZD23), National Natural Science Foundation of China (Grant No. 52271297), National Natural Science Foundation of China (Grant No. 52071303), Shandong Provincial Natural Science Foundation (Grant No. ZR2022ME002), National Natural Science Foundation of China (Grant No. U22A20216), Taishan Scholars Program of Shandong Province (No. ts20190914), Qingdao Postdoctoral Program Grant (Grant No. QDBSH20220201015), Fundamental Research Funds for the Central Universities (Gant No. 202313031) and Chinese Scholarship Council (CSC, China).

Reference

A. Aubault, M. Alves, A. Sarmento, D. Roddier, A. Peiffer, 2011. Modeling of an oscillating water column on the floating foundation WindFloat, in: Proc. Int. Conf. Offshore Mech. Arct. Eng. - OMAE. 235. https://doi.org/10.1115/OMAE2011-49014.

Arany, L., Bhattacharya, S., 2018. Simplified load estimation and sizing of suction anchors for spar buoy type floating offshore wind turbines. Ocean Eng. 159, 348–357. https://doi.org/10.1016/j.oceaneng.2018.04.013

Ansys, 2020. Aqwa Theory Manual Release 2020 R2, USA, Ansys Inc., Canonsburg, USA.

Aboutalebi, P., M'zoughi, F., Garrido, I., Garrido, A.J., 2021a. Performance analysis on the use of oscillatingwater column in barge-based floating offshore wind turbines. Mathematics 9, 1–22. https://doi.org/10.3390/math9050475

Aboutalebi, P., M'zoughi, F., Martija, I., Garrido, I., Garrido, A.J., 2021b. Switching control strategy for oscillating water columns based on response amplitude operators for floating offshore wind turbines stabilization. Appl. Sci. 11. https://doi.org/10.3390/app11115249

Abazari, A., 2023. Dynamic Response of a Combined Spar-Type FOWT and OWC-WEC by a Simplified Approach 4, 67–77. https://doi.org/10.22044/rera.2022.11768.1109

Chen M, Wang R, Xiao P, 2020. Numerical analysis of a floating semi-submersible wind turbine integrated with a point absorber wave energy convertor[C]//The 30th International Ocean and Polar Engineering Conference. OnePetro.

Cong, P., Teng, B., Bai, W., Ning, D., Liu, Y., 2021. Wave power absorption by an oscillating water column (OWC) device of annular cross-section in a combined wind-wave energy system. Appl. Ocean Res. 107. https://doi.org/10.1016/j.apor.2020.102499

Ekerhovd, I., Chen, M., Taylor, P.H., Zhao, W., 2021. Numerical study on gap resonance coupled to vessel motions relevant to side-by-side offloading. Ocean Eng. 241, 110045. https://doi.org/10.1016/j.oceaneng.2021.110045

Falcão, A.F.O., Henriques, J.C.C., Cândido, J.J., 2012. Dynamics and optimization of the OWC spar buoy wave energy converter. Renew. Energy 48, 369–381. https://doi.org/10.1016/j.renene.2012.05.009

Gaertner, E., Rinker, J., Sethuraman, L., Zahle, F., Anderson, B., Barter, G., Abbas, N., Meng, F., Bortolotti, P., Skrzypinski, W., Scott, G., Feil, R., Bredmose, H., Dykes, K., Shields, M., Allen, C., Viselli, A., 2020. IEA Wind - Offshore Reference Wind - 15MW.

Ghafari, H.R., Ghassemi, H., Neisi, A., 2022. Power matrix and dynamic response of the hybrid Wavestar-DeepCwind platform under different diameters and regular wave conditions. Ocean Eng. 247. https://doi.org/10.1016/j.oceaneng.2022.110734

Hu, J., Zhou, B., Vogel, C., Liu, P., Willden, R., Sun, K., Zang, J., Geng, J., Jin, P., Cui, L., Jiang, B., Collu, M., 2020. Optimal design and performance analysis of a hybrid system combing a floating wind platform and wave energy converters. Appl. Energy 269. https://doi.org/10.1016/j.apenergy.2020.114998

Homayoun, E., Ghassemi, H., Ghafari, H., 2019. Power Performance of the Combined Monopile Wind Turbine and Floating Buoy with Heave-Type Wave Energy Converter. Polish Marit. Res. 26, 107–114. https://doi.org/10.2478/pomr-2019-0051

Kamarlouei, M., Gaspar, J.F., Calvario, M., Hallak, T.S., Mendes, M.J.G.C., Thiebaut, F., Guedes Soares, C., 2020. Experimental analysis of wave energy converters concentrically attached on a floating offshore platform. Renew. Energy 152, 1171–1185. https://doi.org/10.1016/j.renene.2020.01.078

Konispoliatis, D.N., Katsaounis, G.M., Manolas, D.I., Soukissian, T.H., Polyzos, S., Mazarakos, T.P., Voutsinas, S.G., Mavrakos, S.A., 2021. Refos: A renewable energy multi-purpose floating offshore system. Energies 14. https://doi.org/10.3390/en14113126

Kamarlouei, M., Gaspar, J.F., Calvario, M., Hallak, T.S., Mendes, M.J.G.C., Thiebaut, F., Guedes Soares, C., 2022. Experimental study of wave energy converter arrays adapted to a semi-submersible wind platform. Renew. Energy 188, 145–163. https://doi.org/10.1016/j.renene.2022.02.014

Khatibani, M.J., Ketabdari, M.J., 2022. Numerical modeling of an innovative hybrid wind turbine and WEC systems performance: A case study in the Persian Gulf. J. Ocean Eng. Sci. https://doi.org/10.1016/j.joes.2022.05.008

Lee, H., Poguluri, S.K., Bae, Y.H., 2018. Performance analysis of multiplewave energy converters placed on a floating platform in the frequency domain. Energies 11. https://doi.org/10.3390/en11020406

Li, L., Gao, Y., Yuan, Z., Day, S., Hu, Z., 2018. Dynamic response and power production of a floating integrated wind, wave and tidal energy system. Renew. Energy 116, 412–422. https://doi.org/10.1016/j.renene.2017.09.080

Li, Y., Ong, M.C., Wang, K., Li, L., Cheng, Z., 2022. Power performance and dynamic responses of an integrated system with a semi-submersible wind turbine and four torus-shaped wave energy converters. Ocean Eng. 259. https://doi.org/10.1016/j.oceaneng.2022.111810

Li, Y., Liu, S., Xu, C., Li, D., Shi, H., 2022. Experimental study on the cylindrical oscillating water column device. Ocean Eng. 246. https://doi.org/10.1016/j.oceaneng.2022.110523

Li, M., Wu, R., Wu, B., Yang, Z., Li, G., 2022. Hydrodynamic performance and optimization of a pneumatic type spar buoy wave energy converter. Ocean Eng. 254. https://doi.org/10.1016/j.oceaneng.2022.111334

Muliawan, M.J., Karimirad, M., Moan, T., 2013a. Dynamic response and power performance of a combined Spar-type floating wind turbine and coaxial floating wave energy converter. Renew. Energy 50, 47–57. https://doi.org/10.1016/j.renene.2012.05.025

Muliawan, M.J., Karimirad, M., Gao, Z., Moan, T., 2013b. Extreme responses of a combined spar-type floating wind turbine and floating wave energy converter (STC) system with survival modes. Ocean Eng. 65, 71–82. https://doi.org/10.1016/j.oceaneng.2013.03.002

Oikonomou, C.L.G., Gomes, R.P.F., Gato, L.M.C., 2021. Unveiling the potential of using a spar-buoy oscillating-water-column wave energy converter for low-power stand-alone applications. Appl. Energy 292. https://doi.org/10.1016/j.apenergy.2021.116835

Perez-Collazo, C., Pemberton, R., Greaves, D., Iglesias, G., 2019. Monopile-mounted wave energy converter for a hybrid wind-wave system. Energy Convers. Manag. 199. https://doi.org/10.1016/j.enconman.2019.111971

Rony J S, Karmakar D, 2022. Coupled Dynamic Analysis of Hybrid Offshore Wind Turbine and Wave Energy Converter. J. Offshore Mech. Arct. Eng., 144. https://doi.org/10.1115/1.4052936

Ren, N., Ma, Z., Shan, B., Ning, D., Ou, J., 2020. Experimental and numerical study of dynamic responses of a new combined TLP type floating wind turbine and a wave energy converter under operational conditions. Renew. Energy 151, 966–974. https://doi.org/10.1016/j.renene.2019.11.095

Ren, N., Ma, Z., Fan, T., Zhai, G., Ou, J., 2018. Experimental and numerical study of hydrodynamic responses of a new combined monopile wind turbine and a heave-type wave energy converter under typical operational conditions. Ocean Eng. 159, 1–8. https://doi.org/10.1016/j.oceaneng.2018.03.090

Sarmiento, J., Iturrioz, A., Ayllón, V., Guanche, R., Losada, I.J., 2019. Experimental modelling of a multi-use floating platform for wave and wind energy harvesting. Ocean Eng. 173, 761–773. https://doi.org/10.1016/j.oceaneng.2018.12.046

Si, Y., Chen, Z., Zeng, W., Sun, J., Zhang, D., Ma, X., Qian, P., 2021. The influence of power-take-off control on the dynamic response and power output of combined semi-submersible floating wind turbine and point-absorber wave energy converters. Ocean Eng. 227. https://doi.org/10.1016/j.oceaneng.2021.108835

Wang, Y., Zhang, L., Michailides, C., Wan, L., Shi, W., 2020. Hydrodynamic response of a combined wind-wave marine energy structure. J. Mar. Sci. Eng. 8. https://doi.org/10.3390/JMSE8040253

Wang, Y., Shi, W., Michailides, C., Wan, L., Kim, H., Li, X., 2022. WEC shape effect on the motion response and power performance of a combined wind-wave energy converter. Ocean Eng. 250. https://doi.org/10.1016/j.oceaneng.2022.111038

Wan, L., Ren, N., Zhang, P., 2020. Numerical investigation on the dynamic responses of three integrated concepts of offshore wind and wave energy converter. Ocean Eng. 217. https://doi.org/10.1016/j.oceaneng.2020.107896

Yue, M., Liu, Q., Li, C., Ding, Q., Cheng, S., Zhu, H., 2020. Effects of heave plate on dynamic response of floating wind turbine Spar platform under the coupling effect of wind and wave. Ocean Eng. 201. https://doi.org/10.1016/j.oceaneng.2020.107103

Yan, S., Ma, Q., Cheng, X., 2012. Numerical investigations on transient behaviours of two 3-D freely floating structures by using a fully nonlinear method. J. Mar. Sci. Appl. 11, 1–9. https://doi.org/10.1007/s11804-012-1099-0

Yan, S., Ma, Q.W., Cheng, X., 2011. Fully Nonlinear Hydrodynamic Interaction Between Two 3D Floating Structures In Close Proximity. Int. J. Offshore Polar Eng. 21.

Zhu, H., Hu, C., Sueyoshi, M., Yoshida, S., 2020. Integration of a semisubmersible floating wind turbine and wave energy converters: an experimental study on motion reduction. J. Mar. Sci. Technol. 25, 667–674. https://doi.org/10.1007/s00773-019-00671-y

Zhou, Y., Ning, D., Shi, W., Johanning, L., Liang, D., 2020. Hydrodynamic investigation on an OWC wave energy converter integrated into an offshore wind turbine monopile. Coast. Eng. 162. https://doi.org/10.1016/j.coastaleng.2020.103731

Zhao, C., Thies, P.R., Ye, Q., Lars, J., 2021. System integration and coupled effects of an OWT/WEC device. Ocean Eng. 220. https://doi.org/10.1016/j.oceaneng.2020.108405

Zhang, D., Chen, Z., Liu, X., Sun, J., Yu, H., Zeng, W., Ying, Y., Sun, Y., Cui, L., Yang, S., Qian, P., Si, Y., 2022. A coupled numerical framework for hybrid floating offshore wind turbine and oscillating water column wave energy converters. Energy Convers. Manag. 267. https://doi.org/10.1016/j.enconman.2022.115933